AIP | Applied Physics Letters

Origin and control of magnetic exchange coupling in between focused electron beam deposited cobalt nanostructures

E. Nikulina, O. Idigoras, J. M. Porro, P. Vavassori, A. Chuvilin, and A. Berger

Citation: Applied Physics Letters **103**, 123112 (2013); doi: 10.1063/1.4821034
View online: http://dx.doi.org/10.1063/1.4821034
View Table of Contents: http://scitation.aip.org/content/aip/journal/apl/103/12?ver=pdfcov
Published by the AIP Publishing

Origin and control of magnetic exchange coupling in between focused electron beam deposited cobalt nanostructures

E. Nikulina,[1] O. Idigoras,[1] J. M. Porro,[1] P. Vavassori,[1,2] A. Chuvilin,[1,2,a)] and A. Berger[1]
[1]*CIC nanoGUNE Consolider, Tolosa Hiribidea 76, 20018 Donostia-San Sebastian, Spain*
[2]*Ikerbasque, Basque Foundation for Science, Alameda Urquijo 36-5, 48011 Bilbao, Spain*

(Received 3 July 2013; accepted 28 August 2013; published online 18 September 2013)

We demonstrate the existence and control of inter-particle magnetic exchange coupling in densely packed nanostructures fabricated by focused electron beam induced deposition. With Xe beam post-processing, we have achieved the controlled reduction and eventual elimination of the parasitic halo-like cobalt deposits formed in the proximity of intended nanostructures, which are the identified source of the magnetic exchange coupling. The elimination of the halo-mediated exchange coupling is demonstrated by magnetic measurements using Kerr microscopy on Co pillar arrays. Electron microscopy studies allowed us to identify the mechanisms underlying this process and to verify the efficiency and opportunities of the described nano-scale fabrication approach. © *2013 AIP Publishing LLC*. [http://dx.doi.org/10.1063/1.4821034]

During the last years, focused electron beam induced deposition (FEBID) has become a very attractive process for the fabrication and prototyping of nanostructures.[1–3] This technique can be an advantageous alternative to other types of nanofabrication, due to its one-step nature, making it relatively simple, flexible, and fast. Besides these important practical advantages, FEBID has a potential to fabricate extremely small nanostructures. Nowadays, the deposition resolution demonstrated for the FEBID process reaches 3 nm on a bulk substrate[4] and even below 1 nm in a transmission electron microscope on a thin film.[5] Capability of FEBID to fabricate 3-dimensional structures on the nano-scale has been also demonstrated.[6,7]

The FEBID process utilizes a highly focused electron beam, usually from an electron microscope, for the purpose of patterning surfaces of bulk or thin film substrates in the presence of a suitable gas precursor. Hereby, the secondary electrons (SEs) generated by the primary electron beam interact with the precursor molecules adsorbed on the substrate and decompose the precursor into volatile and non-volatile components. The latter then forms a deposit on the substrate in the region under the primary electron beam illumination, whose positioning can then be used to fabricate predefined shapes.[1–3]

Among the materials that can be deposited by FEBID, cobalt (Co) became particularly interesting, thanks to the exceptionally high purity of the deposit (up to 95 atomic percent of Co)[8] and well preserved functional properties, such as magnetic moment, ferromagnetic order, and electrical conductivity.[6–20] In recent years, a number of papers have been published demonstrating that Co FEBID can indeed be used to fabricate functional devices, such as nano-Hall sensors,[11,15,17] magnetic force microscopy (MFM) tips,[6,9] free standing conducting bridges,[6] and domain wall-based devices.[7,13,20] In particular, up-standing magnetic nanopillars or nanocylinders attract considerable scientific and technological interest due to their potential application for storage media, sensing, biomedicine, and model systems for studying magnetostatic interactions and frustration, which are receiving remarkable interest.[21] As a consequence, substantial efforts have been devoted to achieve their controlled synthesis as well as a theoretical understanding of their magnetic behavior.

Given the industrial need and trend towards the fabrication of densely packed functional nanostructures, the resolution of FEBID and its underlying processes have crucial importance. It is known that in FEBID, mainly secondary electrons participate in the precursor molecule dissociation.[1–3] Two main types of SEs can be distinguished, namely, the SE_I, generated near the surface by primary electrons, leading to the fabrication of the main deposit and SE_{II}, generated by highly energetic back-scattered electrons (BSEs), leading to the deposition of a parasitic halo around the main deposit.[3] For a Si bulk substrate the halo can reach up to 7.5 μm at 25 kV in lateral size corresponding to BSE-exit area.[22] Autocatalytic growth and surface activation processes can also cause unintended deposition, further expanding the halo beyond the BSE-exit area.[19] Some authors have claimed that the parasitic halo is poorly conductive and reveals low cobalt concentration.[6,11] Based on these claims, it was assumed that halo-deposits do not have any substantial influence on the FEBID structure functionality and, therefore, not much attention has been paid to this issue up to now. In this work, we show that contrary to these earlier expectations the parasitic Co halo layer in between densely packed FEBID deposited nanostructures actually results in an unintended magnetic exchange coupling. Ga^+ focused ion beam irradiation was previously used for post-processing of FEBID Co structures, resulting in substantial modification of magnetic properties.[20,23] Here we demonstrate that the fabrication of magnetic exchange-decoupled FEBID nanostructures can be achieved by applying a Xe-ion milling post-deposition treatment. Hereby, the efficiency of the Xe post-processing has been demonstrated by means of scanning and scanning transmission electron microscopy (SEM and STEM), energy dispersive X-ray spectroscopy

a)Electronic mail: a.chuvilin@nanogune.eu

(EDX), and magneto-optical Kerr effect (MOKE) magnetometry in terms of direct functional testing.

Focused electron beam induced deposition of cobalt nanostructures was performed in a Helios NanoLab™ DualBeam™ (FEI, Netherlands) system equipped with a Schottky field-emission electron gun and an integrated gas injection system (GIS). Complementary to the standard dual beam configuration, this machine is equipped with a third ion gun IQE 12/38 (SPECS Surface Nano Analysis GmbH, Germany). Co nanostructures were initially fabricated by FEBID process, using the following deposition parameters: background vacuum $= 7 \times 10^{-5}$ Pa, precursor gas pressure $= 8 \times 10^{-4}$ Pa, and sample to GIS-tube distance $= 50\,\mu$m. The electron beam conditions were selected for each specific deposit geometry (see below). An example of thus deposited structure can be seen in the SEM image, shown as an inset in Fig. 1. As shown schematically in Fig. 1, the intended deposition process is accompanied by the formation of an unintended halo surrounding the main Co structures. In order to eliminate this halo we apply a post-treatment consisting of etching by a broad Xe ion beam. Xe-beam conditions are as follows: accelerating voltage = 1 kV, beam current ~ 100 nA, and beam diameter about 300 μm. At this low voltage (1 kV) the Xe ion beam provides a gentle milling with minimal structural damage, while the rather high current density provides a sufficient ion dose rate for efficient etching. Xe-milling was performed perpendicular to the substrate surface to minimize the shape modification of the intended FEBID structures. The overall two-step fabrication approach consisting of cobalt FEBID and subsequent Xe ion milling is schematically represented in Fig. 1.

In order to prove the efficiency and reveal the limitations of Xe ion milling for halo elimination, several test arrays of Co nanowires were fabricated (beam voltage = 25 kV, beam current = 2.7 nA, dwell time = 1 μs, pitch = 5 nm, and a total deposition time per nanowire of 2 s) and irradiated by the Xe ion beam, systematically changing the ion dose in the range from zero up to 170 mC/cm^2 (Ref. 24). The specific FEBID fabricated nanowires here are 1 μm long, and each set of arrays consists of 6 nanowires deposited with progressively increasing inter-wire distance of 30, 60, 90, 120, and 150 nm. These sets allow the determination of the ultimate inter-structure spacing achievable by the here proposed two-step fabrication approach. Figures 2(a) and 2(c) show SEM images of two sets of these arrays: one as-deposited and the other one after Xe ion beam exposure (85 mC/cm^2), respectively. Cross-sectional STEM images of the nanowires separated by 150 nm (and indicated by the white arrows in Figs. 2(a) and 2(c)) are shown in Figs. 2(b) and 2(d). The cross-sectional images reveal a continuous 4–5 nm thick film in close proximity of the as-deposited nanowire (Fig. 2(b)), which is the halo structure due to unintended deposition. After Xe beam treatment this halo is no longer visible (Fig. 2(d)). Besides the halo removal the Xe ion beam causes a slight reshaping of the prefabricated FEBID structures, given that the main deposit is exposed to the irradiation by the Xe ions as well. As expected the milling rate is anisotropic, i.e., the material is milled away faster in the vertical direction, parallel to the xenon beam, than in the lateral one. This in particular opens the possibility for controlled reshaping by tilting the Xe ion beam relative to the surface. The other possibility demonstrated below is the reduction of the dimensions of the nanostructures beyond the minimum size directly achievable by FEBID. However, the drawback of the broad beam milling is that the reshaping can only be reliably achieved for sufficiently separated structures. The proximity effect is known to occur in FEBID of densely packed structures.[25,26] In our case the coalescence occurs due to re-deposition of the material sputtered by the Xe ions during post-treatment. An example of such coalescence can be seen for the two closest lines in Fig. 2(c), which are located on the left-hand side. While there is a clear topographic separation in between those lines prior to the post-processing (Fig. 2(a)), this separation becomes less pronounced after Xe irradiation (Fig. 2(c)).

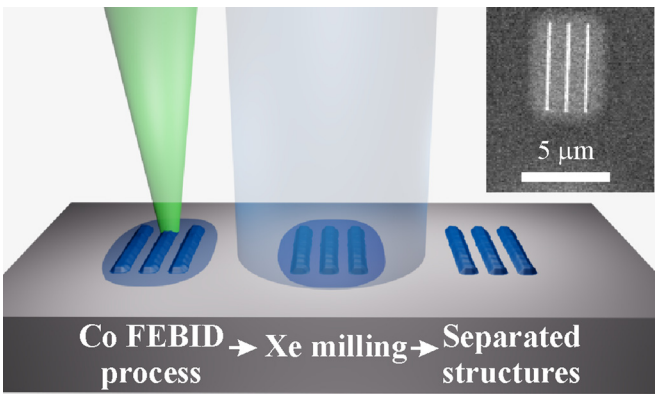

FIG. 1. Schematic of the process sequence resulting in magnetically separated Co FEBID structures. Left to right: the desired Co structures are fabricated utilizing a focused electron beam; subsequently, the as-deposited structures are irradiated by a broad low energy Xe ion beam, leading to uniform surface layer removal; the resulting structures are slightly reduced in size, but the unintended halo-like deposition is eliminated. The inset shows a SEM image of as fabricated FEBID Co nanowires with the parasitic cobalt halo around them.

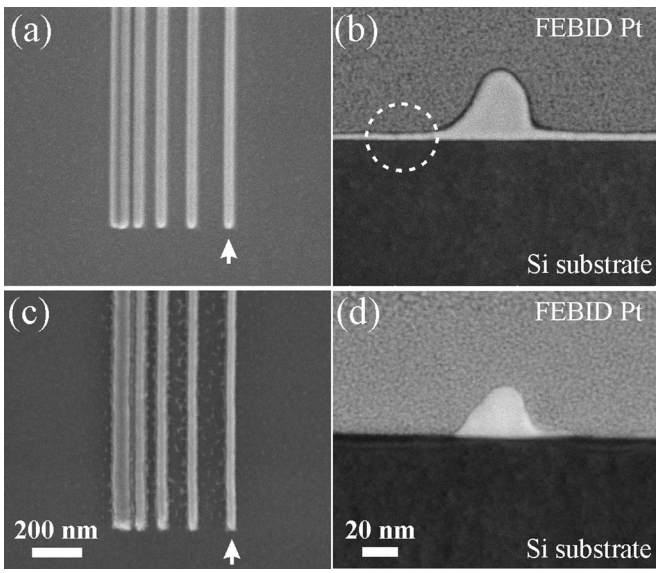

FIG. 2. SEM images of FEBID Co nanowire arrays (viewed at 30° tilt) and corresponding STEM cross-section images (Helios) from the Co nanowires indicated by the white arrows: structures as-deposited (a), (b) and after Xe ion post-treatment using a dose of 85 mC/cm^2 (c), (d). The white dotted circle in (b) indicates the location of the halo in close proximity of the main Co deposit.

Taking these effects into consideration, we applied the Xe ion-milling strategy to the fabrication of 2-dimensional arrays of up-standing cobalt nanopillars. This type of structures possesses vertical magnetic shape anisotropy and might be an interesting model system for studying dipolar interactions, provided that there is no exchange coupling between the individual pillars. Pillar arrays of 20×20 elements with a pitch of 250 nm were deposited at the beam energy = 2 keV, beam current = 86 pA, and dwell time- $= 20\,\mu$s. Post-processing consisted of irradiation by 1 keV Xe ion beam with a total dose of 120 mC/cm^2. Figures 3(a) and 3(b) show two arrays: as-deposited and after post-processing. The SEM image of the as-deposited sample (Fig. 3(a)) shows that besides the halo the pillars are connected by small Co bridges along the beam raster direction due to the fast advance of the beam between the raster points. After Xe ion treatment (Fig. 3(b)) both the bridges and the halo have been successfully removed. Besides this effect, which is intended to functionally isolate the magnetic nanostructures, the Xe milling caused a reshaping of the pillars, namely, a shortening due to the Xe ion bombardment from the top and slight thickening due to the resputtering process. Cross-sections of such pillar structures before and after the Xe treatment were carried out in a transmission electron microscope (Titan^{TM} G2 60-300, FEI, Netherlands) at accelerating voltage of 300 kV. STEM cross-sectional images of the surface between the pillars are shown as insets in Figs. 3(a) and 3(b), and they reveal that as-deposited, the parasitic halo is about 9 nm thick, while after Xe milling, its visible thickness is reduced to below 3 nm. Equally important, the halo layer changed its microstructure as a result of the Xe ion treatment, which is reflected in the contrast change clearly observed in the STEM cross-section images. A detailed analysis shows that the as-deposited halo layer is almost pure nanocrystalline cobalt, while the remaining layer after Xe ion treatment is amorphous and has a very low Co content. Thus, one would expect the post-processed halo not to be magnetic anymore and correspondingly not to be able to mediate ferromagnetic inter-particle exchange coupling in between the individual pillars. Overall, we conclude that post-processing by Xe milling leads to the following: (i) Successful elimination of the cobalt parasitic halo formed around the main deposits, (ii) Controlled reshaping of the deposit dimensions, as well as (iii) Coalescence of densely packed nanostructures due to the re-deposition effect.

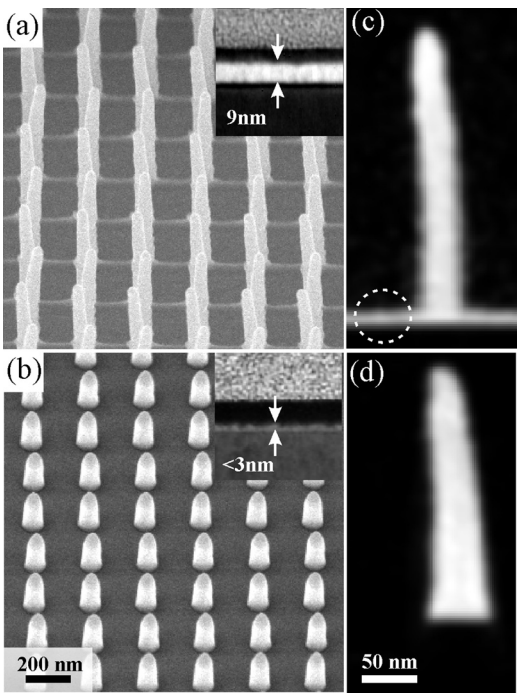

FIG. 3. SEM images of 2-dimensional nanopillar arrays (viewed at an angle), and in insets STEM cross-section images (Titan) showing the thickness of the cobalt halo in between the pillars for as-deposited (a) and Xe ion exposed cases (b). EDX elemental maps show the cobalt distribution in as-deposited (c) and Co FEBID nanopillars Xe-milled at optimal conditions (d). The white dotted circle in (c) indicates the location of the cobalt halo in close proximity to the pillar.

The Xe milling dose can be further optimized in order to minimize reshaping of the structures, while still removing the halo. Figs. 3(c) and 3(d) shows cross-sectional Co EDX maps as a result of such optimization. In the as-deposited case a well-pronounced Co halo appears in close proximity of the pillars (Fig. 3(c)). In contrast, the absence of Co-signal in the EDX map shown in Fig. 3(d), taken after optimal Xe ion exposure, confirms that only a minimal Co content, if any, remains in the severely thinned down halo layer. At the same time the shortening and thickening of the pillars is substantially smaller than observed in Fig. 3(b).

To investigate the impact of Xe milling onto the magnetic properties of nanopillar arrays, their magnetization reversal behavior has been characterized by means of hysteresis loop measurements via MOKE microscopy in polar geometry, i.e., by sweeping a magnetic field parallel to the pillars height. Earlier we have demonstrated the capability of our MOKE microscope based magnetometry approach to measure the magnetization reversal of ultra-small ferromagnetic nanostructures.[18] Here, the hysteresis loops measured for the Co nanopillar arrays are averages of 5 individual hysteresis loop measurements and have been acquired using a ROI of 267×267 pixels, which corresponds to a sample surface area of $4 \times 4\,\mu$m. For the as-deposited Co nanopillar array, shown in Fig. 3(a), the hysteresis loop displays a remnant magnetization close to its saturation value (Fig. 4(a)), which indicates that the array shows the behavior of a magnetic material with strong perpendicular anisotropy and a sufficiently large intra-layer exchange coupling to counterbalance the effect of dipolar coupling, similar to present-day perpendicular recording media.[27] In these FEBID Co-pillars, the perpendicular anisotropy is due to the shape anisotropy caused by the elongated form of the individual nanopillars. The magnetic hysteresis loop measurements on the as-deposited array in Fig. 4(a) furthermore indicate that the magnetization reversal is correlated between different nanopillars and thus dominated by intra-layer exchange coupling, which favors the parallel alignment of the magnetizations in the pillars. This behavior is very different for the case of Co nanopillar arrays, which were post-processed by a Xe ion beam. Here, the magnetization reversal proceeds via a double-step like hysteresis loop (Fig. 4(c)), which exhibits a strongly reduced remnant magnetization. These features suggest that in this case, the magnetization reversal is dominated by the anti-ferromagnetic magnetostatic coupling between

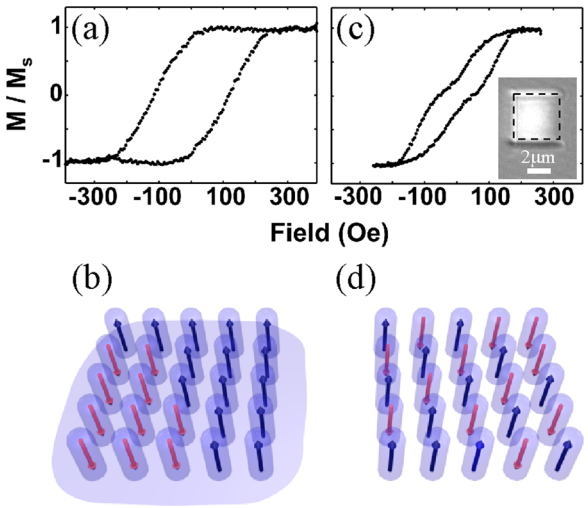

FIG. 4. Out-of-plane MOKE hysteresis loops and schematic sketches of possible magnetization reversal states for 2-dimensional arrays of FEBID cobalt nanopillars: as-deposited structures, having the pillars connected with the cobalt halo (a), (b) and Xe ion exposed with a of dose 120 mC/cm^2 (c), (d). The inset in (c) shows the optical image of the sample, and the dotted square defines the region of interest used for measuring the MOKE loops.

adjacent pillars, while the intra-layer exchange coupling does not play any relevant role anymore. Thus, the pillars here are magnetically disconnected and interact only via the long-range magnetostatic interaction. This demonstrates that the Xe ion milled Co nanopillars are indeed completely separated as far as the intra-layer exchange interaction is concerned and that all functional material modifications that are induced by the unintended halo-like deposition have been removed by the proposed Xe post-processing milling procedure.

In summary, we have shown that magnetic intra-layer exchange coupling in FEBID Co nanostructures plays an important role and needs to be taken into account while designing and fabricating FEBID functional nanodevices. We demonstrate by means of structural as well as functional magnetic characterizations that this intra-layer coupling is caused by a halo-like parasitic cobalt deposition that occurs synchronous with the intended nanostructure fabrication. Comprehensive structural and magnetic investigations furthermore prove that a Xe ion post-treatment is a suitable methodology for the elimination of the parasitic cobalt halo and thus the inter-particle magnetic exchange coupling in between individual nanostructures. We demonstrate that the Xe post-treatment accomplishes this by material removal via sputter processes as well as the dilution of the remaining Co down to concentration levels that do not support magnetic exchange coupling within the halo remnants. The Xe ion procedure furthermore allows for the etching of halo structures in a very gentle way that causes only minimal damage to the FEBID pre-fabricated nanostructures. The unavoidable but tunable structure reshaping that occurs during the Xe ion beam irradiation might also be utilized as a structuring and shaping tool that opens up new perspectives, which go even beyond its application in conjunction with FEBID fabricated structures. From the fundamental point of view, our approach allows for the fabrication of model systems made of arrays of magnetic nanopillars for the study of dipolar interaction effects. Relevant examples are the so-called perpendicular artificial spin ice systems, which are artificially frustrated magnet arrays, consisting of magnetostatically interacting single-domain ferromagnetic units with moments oriented perpendicular to the plane.[21] As far as applications are concerned, our work presents a crucial step forward, because nano-scale applications of FEBID based fabrication will only be relevant, if functional physical properties, such as the magnetization here, can be controlled locally and individually on the nm-scale.

We acknowledge financial support from FEI Company (Netherlands), the Basque Government under the Etortek Program Contract No. IE11-304 and Project PI2012-47, as well as the Spanish Ministry of Science and Education under Project No. MAT2012-36844. O.I. and J.M.P. acknowledge the Basque Government for Fellowships (Nos. BFI09-284 and BFI09-289, respectively).

[1]I. Utke, P. Hoffmann, and J. Melngailis, J. Vac. Sci. Technol. B **26**(4), 1197 (2008).
[2]W. F. van Dorp and C. W. Hagen, J. Appl. Phys. **104**(8), 081301 (2008).
[3]I. Utke, S. Moshkalev, and P. Russel, *Nanofabrication Using Focused Ion and Electron Beams: Principles and Applications* (Oxford University Press, New York, 2012).
[4]L. van Kouwen, A. Botman, and C. W. Hagen, Nano Lett. **9**(5), 2149 (2009).
[5]W. F. van Dorp, B. van Someren, C. W. Hagen, and P. Kruit, Nano Lett. **5**(7), 1303 (2005).
[6]Y. M. Lau, P. C. Chee, J. T. L. Thong, and V. Ng, J. Vac. Sci. Technol. A **20**(4), 1295 (2002).
[7]A. Fernández-Pacheco, L. Serrano-Ramón, J. M. Michalik, M. R. Ibarra, J. M. De Teresa, L. O'Brien, D. Petit, J. Lee, and R. P. Cowburn, Sci. Rep. **3**, 1492 (2013).
[8]A. Fernández-Pacheco, J. M. De Teresa, R. Córdoba, and M. R. Ibarra, J. Phys. D: Appl. Phys. **42**, 055005 (2009).
[9]I. Utke, P. Hoffmann, R. Berger, and L. Scandella, Appl. Phys. Lett. **80**, 4792 (2002).
[10]I. Utke, T. Bret, D. Laub, P. Buffat, L. Scandella, and P. Hoffmann, Microelectron. Eng. **73–74**, 553 (2004).
[11]G. Boero, I. Utke, T. Bret, N. Quack, M. Todorova, S. Mouaziz, P. Kejik, J. Brugger, R. S. Popovic, and P. Hoffmann, Appl. Phys. Lett. **86**, 042503 (2005).
[12]I. Utke, V. Friedli, J. Michler, T. Bret, X. Multone, and P. Hoffmann, Appl. Phys. Lett. **88**, 031906 (2006).
[13]A. Fernández-Pacheco, J. M. De Teresa, R. Córdoba, M. R. Ibarra, D. Petit, D. E. Read, L. O'Brien, E. R. Lewis, H. T. Zeng, and R. P. Cowburn, Appl. Phys. Lett. **94**, 192509 (2009).
[14]A. Fernández-Pacheco, J. M. De Teresa, A. Szkudlarek, R. Córdoba, M. R. Ibarra, D. Petit, L. O'Brien, H. T. Zeng, E. R. Lewis, D. E. Read, and R. P. Cowburn, Nanotechnology **20**, 475704 (2009).
[15]M. Gabureac, L. Bernau, I. Utke, and G. Boero, Nanotechnology **21**, 115503 (2010).
[16]M. Jaafar, L. Serrano-Ramón, O. Iglesias-Freire, A. Fernández-Pacheco, M. R. Ibarra, J. M. De Teresa, and A. Asenjo, Nanoscale Res. Lett. **6**, 407 (2011).
[17]L. Serrano-Ramón, R. Córdoba, L. A. Rodríguez, C. Magén, E. Snoeck, C. Gatel, I. Serrano, M. R. Ibarra, and J. M. De Teresa, ACS Nano **5**(10), 7781 (2011).
[18]E. Nikulina, O. Idigoras, P. Vavassori, A. Chuvilin, and A. Berger, Appl. Phys. Lett. **100**, 142401 (2012).
[19]K. Muthukumar, H. O. Jenschke, R. Valentí, E. Begun, J. Schwenk, F. Porrati, and M. Huth, Beilstein J. Nanotechnol. **3**, 546 (2012).
[20]L. Serrano-Ramón, A. Fernández-Pacheco, M. R. Ibarra, D. Petit, R. P. Cowburn, T. Tyliszczak, and J. M. De Teresa, Eur. Phys. J. B **86**, 97 (2013).
[21]S. Zhang, J. Li, I. Gilbert, J. Bartell, M. J. Erickson, Y. Pan, P. E. Lammert, C. Nisoli, K. K. Kohli, R. Misra, V. H. Crespi, N. Samarth, C. Leighton, and P. Schiffer, Phys. Rev. Lett. **109**(8), 087201 (2012).
[22]L. Reimer, *Scanning Electron Microscopy* (Springer, Berlin, 1985).

[23]J. H. Franken, H. J. M. Swagten, and B. Koopmans, Nat. Nanotechnol. **7**(8), 499 (2012).
[24]Xenon ion beam doses are estimated from the beam spot size, specimen current, and exposure time.
[25]P. A. Crozier, J. Vac. Sci. Technol. B **26**, 249 (2008).
[26]H. Plank, D. A. Smith, T. Haber, P. D. Rack, and F. Hofer, ACS Nano **6**(1), 286 (2012).
[27]A. Berger, B. Lengsfield, and Y. Ikeda, J. Appl. Phys. **99**, 08E705 (2006).